

Lateral Response of 2 x 2 Pile Group Embedded in Cohesive Soil Near Slope

Avinash V. Navale¹, Chandresh H. Solanki², Vishwas A. Sawant³

¹Department of Civil Engineering, Sardar Vallabhbhai National Institute of Technology, Surat, India 395007. (navaleavinash@yahoo.com)

²Department of Civil Engineering, Sardar Vallabhbhai National Institute of Technology, Surat, India 395007. (chandresh1968@yahoo.co.in)

³Department of Civil Engineering, Indian Institute of Technology, Roorkee, India 247667. (vishwas.sawant@ce.iitr.ac.in)

Abstract

This work studies the response of a 2 x 2 pile group near a slope subjected to lateral load. Three-dimensional, non-linear finite element analysis is carried out. The entire code is developed in FORTRAN 90. Bending-dominated pile and pile caps are represented by 20 node elements with quadratic shape function, and shear-dominated soil elements are represented by eight-node elements with linear shape function. Sixteen node interface element of zero thickness is used for stress transfer between pile and soil. The outcome highlights the influence of slope parameters like slope angle and edge distance on the response of the 2 x 2 pile group near a slope. The lateral displacement and maximum bending moments are increased with an increase in slope. However, its effect reduces with an increase in slope distance. The point of zero-shear along the pile's depth shifts deeper with an increase in slope.

Author Keywords. 2 x 2 Pile Group, Slope Angle, Edge Distance, Modified Cam Clay Model, Lateral Load

Type: Research Article

 Open Access  Peer Reviewed  CC BY

1. Introduction

In many situations, the superstructure is subjected to horizontal load. Such as, in tall buildings, transmission towers, and chimneys, wind load governs the design. The drag of the moving vehicles creates the lateral force in bridges. Due to seismic activity, structures experience horizontal force. This lateral force should be transmitted to the ground by the substructure. Mostly pile foundations are used in such cases. In the buildings in a hilly area or abutments of a bridge, the piles are near the slope. The method for analysis and design of laterally loaded piles or pile groups near the slope is still not well established.

Several analytical, numerical, and experimental studies have been published for a single pile subjected to lateral stress on level ground. However, studies on pile groups are limited. Georgiadis et al. (1992) performed a series of tests on the model pile to investigate the response of a pile embedded in soft clay subjected to cyclic lateral loads. The results obtained from these tests were compared with numerically predicted pile responses. Based on the test results, the p-y

relationship was created by considering the impact of the cyclic stress level and the number of load cycles. L. Chen and Poulos (1993) presented a numerical analysis that combined finite and infinite elements to investigate the group effects on the ultimate lateral soil resistance. The results indicated that grouping of piles tends to reduce the pile capacity when the spacing between piles was within practical range. Uncuoglu and Laman (2011) conducted different model tests to study the response of short rigid piles embedded in a two-layer sandy soil under lateral loading. The experimental study was complemented by a numerical study using 3D non-linear finite-element analysis to explore the effects of various parameters such as Young's modulus, dilatancy, and interface behavior. Rollins et al. (2006) performed a computer analysis to back-calculate p multipliers using the data obtained from three full-scale lateral load tests on pile groups in stiff clay. The p multipliers were observed to increase with pile spacing. It was observed that the group capacity was not reduced if the spacing was more significant than about 6.5 times of diameter for leading row piles and 7-8 times of diameter for trailing row piles. They developed the p multiplier versus normalized pile spacing curves. Basu et al. (2009) developed a method to obtain the lateral pile response in multi-layered elastic soil. The displacement fields were used in the study as sums of independent functions that varied in the circumferential, radial, and vertical directions. The notion of minimal potential energy was applied to obtain the governing differential equations for the pile deflections in various soil layers. Analytical results were produced for pile deflection solutions. Soil displacements were obtained using the 1D finite difference method (FDM) approach. The method produced results with an accuracy comparable to that of a 3D finite element analysis (FEA). The required computation time was much lesser than the 3D FEA. Mukherjee and Dey (2019) analyzed the fixed-headed single pile subjected to lateral load in layered soil using the p - y approach. Layered soil was considered as the alternate layer of clay and sand. Due to the complex soil response, an idealized model was used for the analysis. Using OASYS ALP v19.2, soil behavior was explained based on the reported non-linear p - y curves.

If a pile is near a slope, less soil is available on the sloping side to offer passive resistance. If the load direction is in the slope direction, the pile capacity is drastically reduced compared to the horizontal ground case. It is challenging to predict the relative stiffness of the pile-soil system in sloping ground. Limited studies are available in the literature related to the performance of laterally loaded pile or pile groups in the ground with slope. Stewart et al. (1993) studied the piles of a bridge abutment with soft clay experiencing lateral load from soil movement. The stiffness of the soft clay layer, Poisson's ratio, and stiffness of the sand substratum are the essential characteristics. Ng and Zhang (2001) presented a 3D numerical analysis to investigate the influence of sleeved and un-sleeved piles on a cut slope. Due to sleeving, the subgrade reaction has considerably reduced on the sleeved pile segment, and the pile response may considerably increase under small lateral loads. The influence of sleeving on pile response appears to be lessened as broad-spread plastic zones form around the pile under heavy lateral loads. Chae et al. (2004) performed a 3D analysis of a single pile and pile group on flat and 30° sloping ground. In both cases, it was noticed that the lateral resistance is less close to the crest. There is a significant reduction in group efficiency with increasing displacement of piles near the sloping ground. It has also been observed that the depth of the rotation point is not changing with the displacement increase. Muthukumaran et al. (2008) applied a surcharge to the ground in

cohesionless soil and studied its effect on pile response. Different slope angles and relative densities were considered. From the observations, p - y relationships were proposed for different cases. Pourkhosravani & Asakereh, (2013) studied the effect of slopes on single pile when the pile experiences lateral load in cohesive soils using the FLAC 3D program. The authors have found that the 70% increase in slope reduces the lateral load capacity of the pile by 18%. The lateral load capacity of the pile can be increased by increasing the length of the pile. The authors have reported a 55% increase in the lateral load capacity of the pile with a 35% increase in pile length. Muthukkumaran and Begum (2015) conducted an experimental investigation on a single model pile to study the effect of slope on the lateral load capacity of the pile and p - y curves in cohesionless soil. The effect of relative density of soil and length to diameter ratio (L/D) was also investigated. Rathod et al. (2015) analyzed 3 x 3 pile groups using PLAXIS 3D and computed the deflection and maximum bending moment of piles in clay. The comparison of responses in the middle, back, and front rows was presented for two slopes (i) 1V:5H and (ii) 1V:3H under a lateral load. Khati and Sawant (2020a) presented the results of 22 laboratory tests on a laterally loaded single pile embedded in dense sand with 72% relative density.

Three ground slopes, 1V: 1.5H, 1V: 1.75H, and 1V: 2H, were considered, and the pile response in displacement and bending strain was observed for seven different positions of the pile from the crest of the slope. The relationship was proposed to find the lateral load capacity of the pile on the sloped ground at different edge distances for the flexibility factor considered in the study. Khati and Sawant (2020b) extended their work for two piles in series and parallel arrangement embedded in medium sand (relative density 52%). The effect of sloping parameters on pile response was presented from 23 tests considering three ground slopes and four edge distances. Tang & Yang, (2020) performed experiments on a pile group consisting of two piles on steep and weathered rock slopes. The outcome highlighted the influence of slope angle. An analytical solution was proposed for a pile installed on a weathered rock slope.

The literature study reveals that the work reported in a pile or pile group near the slope under the action of lateral load is minimal. This study studied the response of a 2 x 2 square pile group near the ground on a slope. The horizontal load is applied in increments, and the effect of slope angle and edge distance is investigated. This is a three-dimensional soil structure interaction problem. The entire code is written in FORTRAN 90 to conduct finite element analysis. Modified Cam clay model represents soil non-linearity and plasticity. The response is obtained in terms of lateral displacement and bending moments. The design of a laterally loaded pile is mainly governed by the displacement criterion than the strength criterion. Different allowable lateral displacements are suggested in the literature depending on the purpose of structure. It is from 5 mm (IS 2911 (Part 4) -1985 (Reaffirmed 2010)) to 20% of the diameter Narasimha et al. (1998). The diameter of the pile used in this study is 1m. Hence, the ultimate loads are calculated at the displacement of 5 mm and 200 mm.

2. Materials and Methods

2.1. Finite Element Model

The system under consideration consists of a pile and pile cap of reinforced concrete surrounded by soil. 3D geometric finite element model represents it. The complete code is written in FORTRAN 90, and the pile behavior is bending-dominated. Hence, 20 node elements with

quadratic shape functions are used in the model pile and pile cap. The soil is predominantly subjected to shear stresses. In general, eight-node elements with linear shape functions represent soil. Sixteen node interface elements with zero thickness are employed to ensure the stress transfer between the ground and the pile. The normal and tangential stiffness of these elements is selected such that relative slip between the pile and soil is possible, but gapping is prohibited. Where the 16 node interface element is adjoined to 8 node soil element horizontally, a 12 node soil element is placed in between to ensure displacement continuity. Similarly, a 9-node soil element connects 12 node soil elements and eight-node soil elements vertically. The shape functions of 9 nodes and 12 node elements are obtained from the shape functions of 20 node elements by degradation technique.

2.2. Non-linear Behavior of Soil

The behavior of the soil is highly non-linear. If simple elastoplastic models represent soil, features like softening and hardening after yielding cannot be captured. Moreover, they predict excessive dilatancy if the associative flow rule (yield function and plastic potential function are the same) is used. Hence, the modified cam clay criterion, one of the critical state models, is used to represent soil in the present study. Stress invariants are independent of the direction chosen for the coordinate axes. Hence, the stress invariants; mean effective stress, p' , deviatoric stress, J and Lode's angle, θ are used instead of principal stresses to represent the modified Cam clay criterion. The stress invariants can be obtained from the principal stresses as below (Potts and Zdravkovic, 1999).

$$p' = \frac{\sigma_1 + \sigma_2 + \sigma_3}{3} \quad J = \frac{1}{\sqrt{6}} \sqrt{(\sigma_1 - \sigma_2)^2 + (\sigma_2 - \sigma_3)^2 + (\sigma_3 - \sigma_1)^2}$$

$$\text{and } \theta = \tan^{-1} \left(\frac{1}{\sqrt{3}} \left(2 \frac{(\sigma_2 - \sigma_3)}{(\sigma_1 - \sigma_3)} - 1 \right) \right) \quad (1)$$

In the elasto-plastic state, the relation between incremental stresses, $\{\Delta\sigma\}$ and incremental strains $\{\Delta\varepsilon\}$ is given as,

$$\{\Delta\sigma\} = [D]_{ep} \{\Delta\varepsilon\} \quad (2)$$

where, $[D]_{ep}$ is the elastoplastic constitutive matrix.

$$[D]_{ep} = [D] - \frac{[D] \left\{ \frac{\partial P}{\partial \sigma} \right\} \left\{ \frac{\partial F}{\partial \sigma} \right\}^T [D]}{A + \left\{ \frac{\partial F}{\partial \sigma} \right\}^T [D] \left\{ \frac{\partial P}{\partial \sigma} \right\}} \quad (3)$$

Where, [D] = elastic constitutive matrix, P and F are the plastic potential and yield functions, respectively. For material with perfect plasticity, $A = 0$ (Potts and Zdravkovic, 1999). Using the chain rule, the flow vector, $a = \{\partial F/\partial \sigma\}$, can be written as:

$$a = \frac{\partial F}{\partial p'} \frac{\partial p'}{\partial \sigma} + \frac{\partial F}{\partial J} \frac{\partial J}{\partial \sigma} + \frac{\partial F}{\partial \theta} \frac{\partial \theta}{\partial \sigma} \quad (4)$$

Nayak and Zienkiwicz (1972) transformed the yield criterion into a more straightforward form to simplify calculations. Furthermore, Viladkar et al., (1995) converted some yield requirements into practical forms for straightforward implementation in finite element codes. Using the approach proposed by Nayak and Zienkiwicz (1972) and Viladkar et al. (1995), the yield function is represented as,

$$a = C_1 a_1 + C_2 a_2 + C_3 a_3 \quad (5)$$

where, $C_1 = \frac{\partial F}{\partial p'}$; $C_2 = \frac{\partial F}{\partial J}$; $C_3 = \frac{\partial F}{\partial \theta}$ and $a_1 = \frac{\partial p'}{\partial \sigma}$; $a_2 = \frac{\partial J}{\partial \sigma}$; $a_3 = \frac{\partial \theta}{\partial \sigma}$

$$a_1 = \frac{\partial p'}{\partial \sigma} = \frac{1}{3} [1 \ 1 \ 1 \ 0 \ 0 \ 0]^T$$

$$a_2 = \frac{\partial J}{\partial \sigma} = \frac{1}{2J} [\sigma_x - p' \ \sigma_y - p' \ \sigma_z - p' \ 2\tau_{xy} \ 2\tau_{yz} \ 2\tau_{zx}]^T$$

$$a_3 = \frac{\partial \theta}{\partial \sigma} = \frac{\sqrt{3}}{2J^3 \cos 3\theta} \left(3 \frac{J_3}{J} \frac{\partial J}{\partial \sigma} - \frac{\partial J_3}{\partial \sigma} \right) \quad (6)$$

where, $J_3 = \begin{vmatrix} \sigma_x - p' & \tau_{xy} & \tau_{zx} \\ \tau_{xy} & \sigma_y - p' & \tau_{yz} \\ \tau_{zx} & \tau_{yz} & \sigma_z - p' \end{vmatrix}$

2.3. Modified Cam clay criterion

It is presumable that during draining isotropic compression, the object moves along a plane trajectory comprising a brand-new consolidation line and a collection of swelling lines. Virgin consolidation lines are assumed to be straight in $v - \ln p'$ space governed by an equation $v - \lambda \ln p' = v_1$. Similarly, swelling lines follow the equation $v - \kappa \ln p' = v_s$. The values of λ , κ and v_1 are characteristics of the particular type of clay. v_s is different for each swelling line. The bulk modulus of soil can be related to the slope of the swelling line.

$$K = \frac{d p'}{d \varepsilon_v^e} = \frac{v p'}{\kappa} \quad (7)$$

The yield function of the modified Cam clay model can be expressed in terms of stress invariants as

$$\left(\frac{J}{p'g(\theta)}\right)^2 - \left(\frac{p_0}{p'} - 1\right) = 0 \quad \text{where} \quad g(\theta) = \frac{\sqrt{3} \sin \phi_{cs}}{\sqrt{3} \cos \theta + \sin \theta \sin \phi_{cs}} \quad (8)$$

where, p_0 = value of p' at the intersection of the current swelling line with virgin consolidation line and ϕ_{cs} is critical state angle of shearing resistance. The projection of these curves on $J - p'$ plane is shown in **Figure 1**, where M_J is the slope of the critical state line (CSL). Model-specific variables (C_1, C_2, C_3) of the flow vector for the modified cam clay model can be computed below.

$$C_1 = \frac{\partial F}{\partial p'} = \frac{1}{p'} \left[1 + \frac{p_0}{p'} \right] ; \quad C_2 = \frac{\partial F}{\partial J} = 2J \left(\frac{1}{p'g(\theta)} \right)^2 \quad (9)$$

$$C_3 = \frac{\partial F}{\partial \theta} = -2 \left(\frac{J}{p'g(\theta)} \right)^2 \frac{1}{g(\theta)} \frac{\sqrt{3} \sin \phi_{cs} (\sqrt{3} \sin \theta - \cos \theta \sin \phi_{cs})}{(\sqrt{3} \cos \theta + \sin \theta \sin \phi_{cs})^2}$$

The parameter p_0 , connected to the plastic volumetric strain, regulates hardening and softening. Increments in the yield surface dp_0 and hardening parameter A are given by-

$$dp_0 = \frac{v p_0}{\lambda - \kappa} d\varepsilon_v^p \quad \text{and} \quad A = -\frac{1}{\Lambda} \frac{\partial F}{\partial p_0} dp_0 = \frac{p_0}{p_0} \frac{v}{\lambda - \kappa} C_1 \quad (10)$$

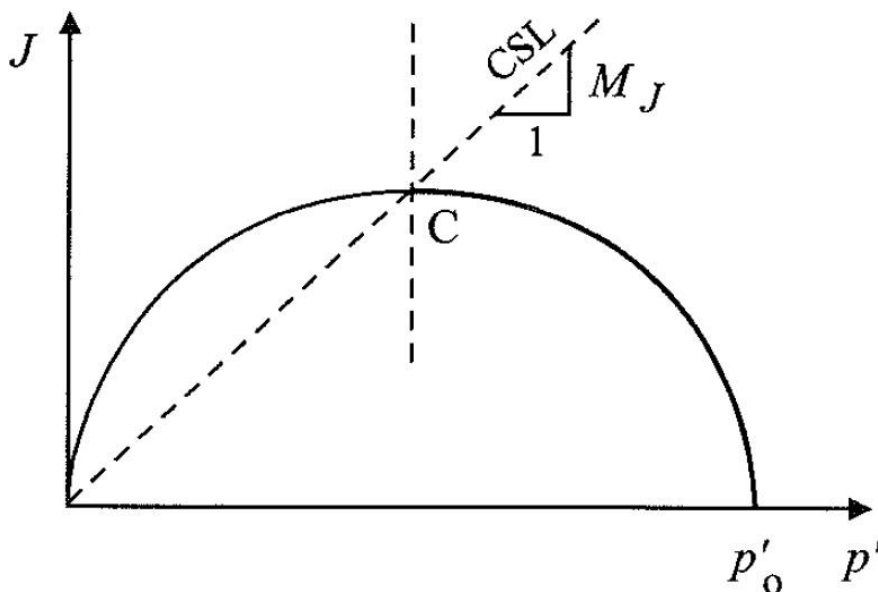


Figure 1: Projection of yield surface of the modified cam clay model on $J - p'$ plane

2.4. Non-linear Algorithm to Calculate Displacement Due to Static Load

The static load is divided into ten equal parts, each part is applied separately, and the steps below are followed for each part. The stiffness matrix, $[K]$ is maintained constant throughout the process. The algorithm to be used after applying each tenth of the load for non-linear analysis is given below.

For the first cycle of each equal part, apply the one-tenth value of the total load as incremental load $\{\Delta F\}$. For the subsequent cycles, apply $\{\Delta F\}$ obtained in step (6) as incremental load. The following equation is solved to obtain incremental displacement $\{\Delta u\} = [K]^{-1} \{\Delta F\}$.

Incremental displacement, Δq , is to be added to the displacement obtained in the previous increment u_{i-1} and the displacement for the i th increment is obtained as

$$\{q\}_i = \{q\}_{i-1} + \{\Delta q\}_i.$$

The value of the number of yielded elements, y_e , is equal to zero.

The value of the number of yielded points, y_p , is set to zero for each element.

From the global incremental displacement vector Δu , the elemental incremental displacement vector $\{\Delta \delta\}$ is to be selected.

The incremental stress, $\{\Delta \sigma\}$ and the total stress for the i th increment, $\{\sigma_i\}$, for all 27 Gauss points are obtained using the relations given below:

$$\{\Delta \sigma\} = [D] [B] \{\Delta \delta\} \text{ and } \{\sigma_i\} = \{\sigma_{i-1}\} + \{\Delta \sigma\}$$

where, $\{\sigma_{i-1}\}$ is the total stress at $i-1$ th iteration. $\{\sigma_i\}$ is checked against yield stress. The next yield point is considered if the Gauss point under consideration is not yielded. Otherwise, y_p is set equal to y_p+1 and extra stress than the yield stress. $\{\Delta \sigma\}_{\text{extra}}$ is calculated using the following relation:

$$\{\Delta \sigma\}_{\text{extra}} = [D - D_{ep}] \{\Delta \varepsilon\}$$

The total stress is kept at the yield level by the following equation,

$$\{\sigma_i\} = \{\sigma_i\} - \{\Delta \sigma\}_{\text{extra}}$$

The additional load vector $\{\Delta F\}$ is obtained below and applied in the next iteration.

$$\{\Delta F\}^e = \iiint_V [B]^T \cdot \{\Delta \sigma\}_{\text{ext}} dV$$

Compute the increment in the yield surface dp_0 and hardening parameter A

This procedure is repeated for all Gauss points of the element.

If $y_p > 0$, y_e is set equal to $y_e + 1$.

Step (4) to (6) is repeated for all elements.

If $y_e = 0$, no element is yielded, and the next one-tenth part of the load is applied.

If $y_e > 0$, then convergence is checked using the following criteria:

$$e_d = \left(\sqrt{\sum (q_i)^2} - \sqrt{\sum (q_{i-1})^2} \right) / \sqrt{\sum (q_i)^2}$$

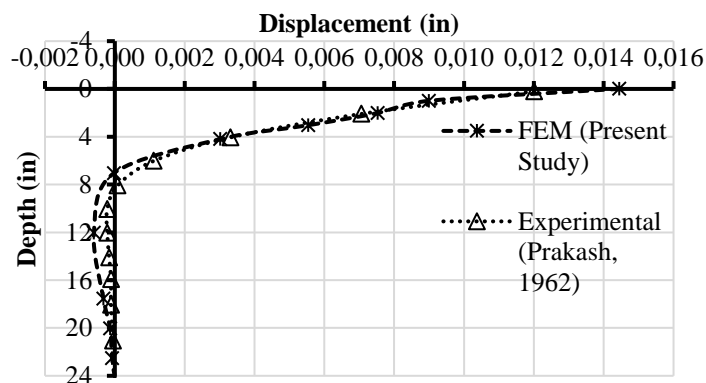
where, e_d = displacement norm, q_i and q_{i-1} are the total displacements at the i th and $i-1$ th iteration.

If the convergence criterion is observed, the next tenth of the load is applied. Else the procedure from step (1) to step (9), is repeated until the convergence of the displacements.

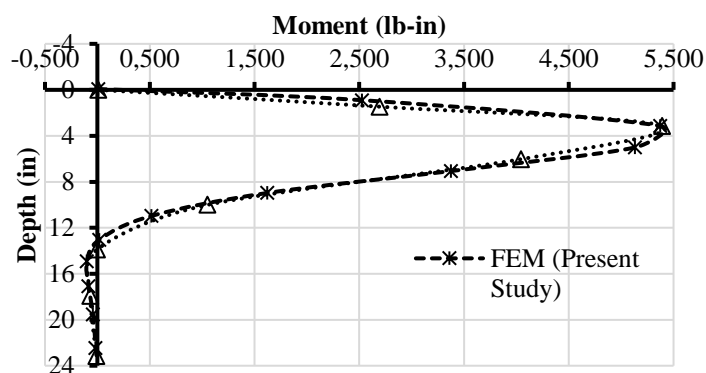
3. Results and Discussion

3.1. Validation

Prakash (1962) conducted an experimental study on a laterally loaded pile embedded in sand. The section of the pile was hollow and circular, with a diameter of 1.6 inches. In numerical modeling, it is converted into the equivalent solid circular section. The equivalent modulus of elasticity of sand is calculated using the relation $E = J\gamma z$ (Terzaghi and Peck 1967), where z is the depth from the surface, γ is the density of soil, and J is the dimensionless parameter whose value is taken as 350. The Poisson's ratio and unit weight of the sand are 0.25 and 18.9 kN/m³, respectively. The boundary below the tip was considered rigid and rough, and the lateral boundary was rigid and smooth. The gapping between the pile and soil was prohibited, but slipping was allowed. The displacements and variation of bending moment obtained experimentally by Prakash (1962) and the proposed software are compared and presented in **Figure 2 (a) and (b)**. The maximum deviation obtained is 10% in displacement and 8% in bending moment. The results show reasonable agreement (**Figure 3**).



(a)



(b)

Figure 2: (a) Validation of displacement with experimental results, and (b) Validation of bending moment with experimental results (Prakash, 1962)

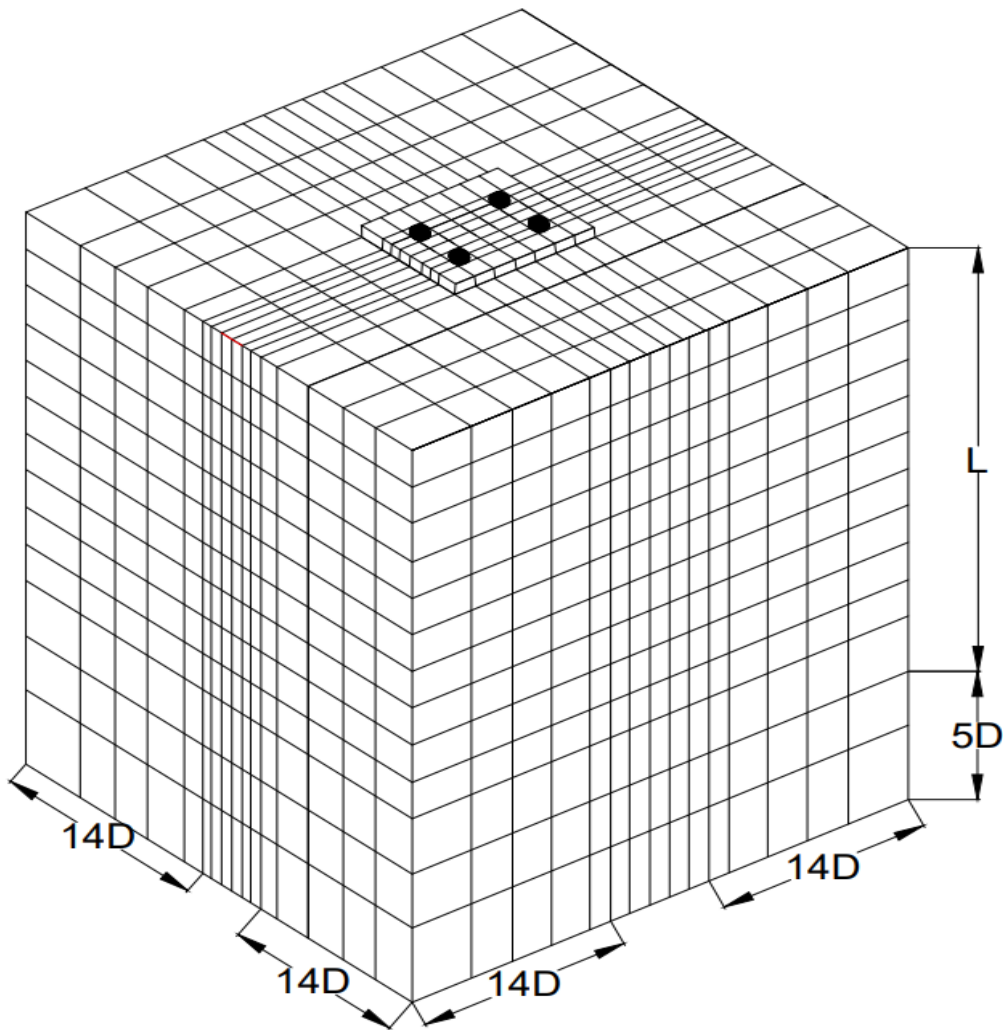


Figure 3: Finite element mesh used for 2 x 2 pile group in horizontal ground

3.2. Parametric Study

As a basis for the analysis of 2 x 2 pile groups in the ground with slope, the analysis of 2 x 2 pile groups in the horizontal ground is carried out first. The finite element mesh is depicted in Figure 3. Piles with length to diameter ratio (L/D) equal to 25 and spacing of $3D$ are used. The properties of pile, soil, and interface elements are mentioned in **Table 1**. After several trials for a horizontal load of 1500 kN, it was noticed that the change in response is negligible if the soil mesh was modeled more than $14D$ from the edge of the pile.

The lateral displacement of the pile group was found at 215.52 mm at the horizontal load of 1500 kN. **Figure 4** shows the bending moment variation along the pile depth for the front (G1) and rear pile (G2). In a square arrangement, the shadowing effect of the stress zone of the pile in one row increases the stresses on the soil in the stress zone of the piles in another row. Hence, a higher bending moment is observed in a rear pile (7284.57 kN-m) than in the front pile (6618.51 kN-m). The ultimate loads corresponding to 5 mm (H_{hor}^{u5}) and 200 mm (H_{hor}^{u200}) displacements are 244.01 kN and 1438.58 kN, respectively.

Elasticity Modulus, E_s	10000 kPa to 40000 kPa
Unit Weight, γ_s	18.5 kN/m ³
Poisson's ratio, μ_s	0.35
Cohesion, c	110 kPa
Angle of internal friction, φ	0
Gradient of compression line, λ	0.14
Gradient of swelling line, κ	0.03
Specific volume,	2.1
p' at the intersection of virgin consolidation line, p_0	60
Pile properties	
Elasticity Modulus, E_p	25 GPa
Pile diameter, D	0.7 m, 0.8 m, 0.9 m and 1.0 m
Poisson's ratio, μ_p	0.25
L/D ratio	10, 15, 20 and 25
Unit Weight, γ_p	25 kN/m ³
s/D ratio	2, 3, 4 and 5
Thickness of Pile cap, t_p	0.55 m
Interface element	
Normal stiffness, K_n	1.0×10^7 kN/m ³
Tangential stiffness, K_s	1100 kN/m ³

Table 1: Properties of piles and soil used for parametric studies
 Soil properties

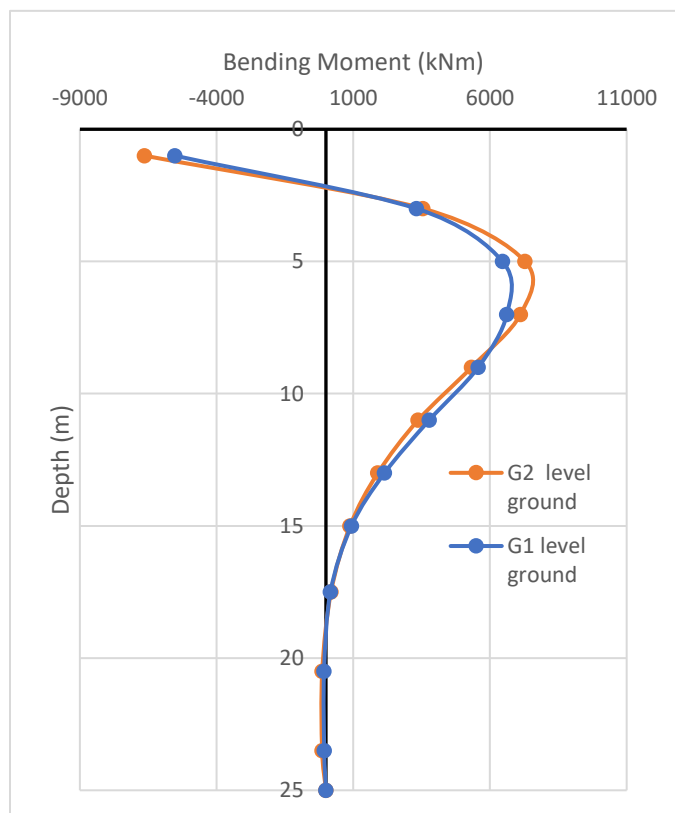


Figure 4: Comparison of bending moment along the depth of pile G1 and G2 in horizontal ground

3.3. Load Displacement Response –

The analysis in the level ground is used as a benchmark for the analysis of 2 x 2 pile groups in the ground with slope. The finite element mesh used for piles in the sloped ground is depicted in **Figure 5**. The effect of slope parameters like slope angle (θ) and edge distance (s) is investigated. Edge distance means the distance between the point where the slope starts and the edge of the pile cap. The direction of application of load and direction of the slope is the same. Four ground slopes - 10° , 20° , 30° , and 40° are considered in the study. The distances considered are zero, $2D$, $5D$, and $9D$. A total of 16 analyses are performed to highlight the effect of slope parameters.

The influence of slope angle on the lateral displacement when the edge distance is zero is shown in **Figure 6** for a 2 x 2 pile group. As the slope angle increases, the soil on the sloping side reduces, and less passive resistance is offered. This yields higher displacements. At the horizontal load of 1500 kN, the displacement increases by 2.63 %, 7.36 %, 14.13 %, and 27.9 % for the slope of 10° , 20° , 30° and 40° respectively. The ultimate load corresponding to 5 mm displacement is decreased by 2.87 %, 6.19 %, 9.67 %, and 12.79 %, whereas the ultimate load corresponding to 200 mm displacement is decreased by 1.43 %, 3.82 %, 6.95 %, and 12.4 % concerning the ultimate load predicted in level ground case.

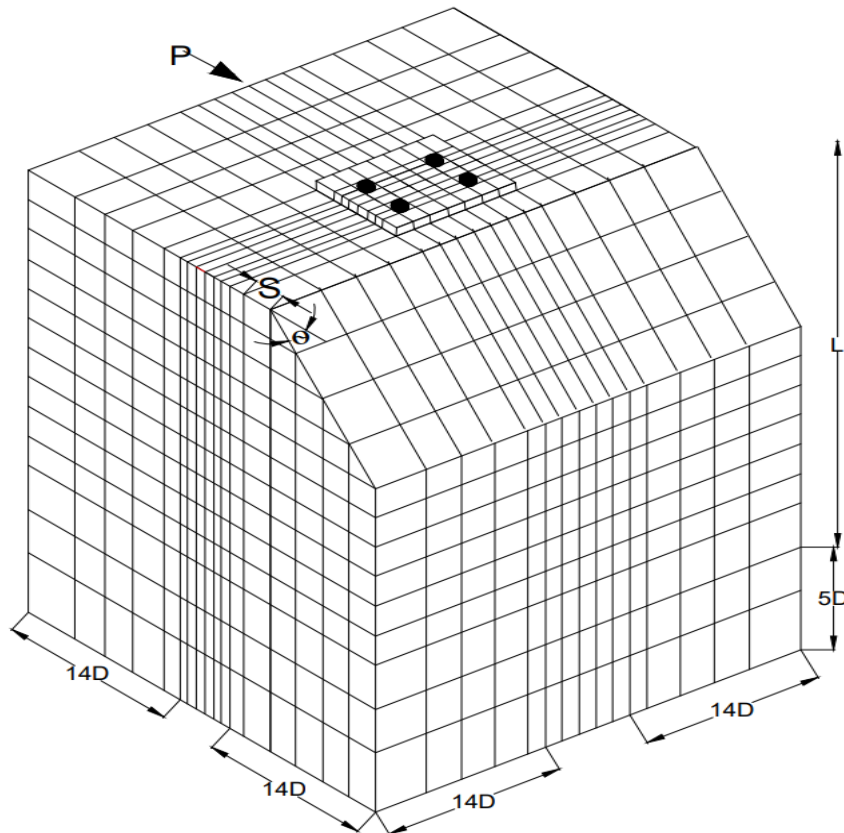


Figure 5: Finite element mesh used for 2 x 2 pile group in ground slope

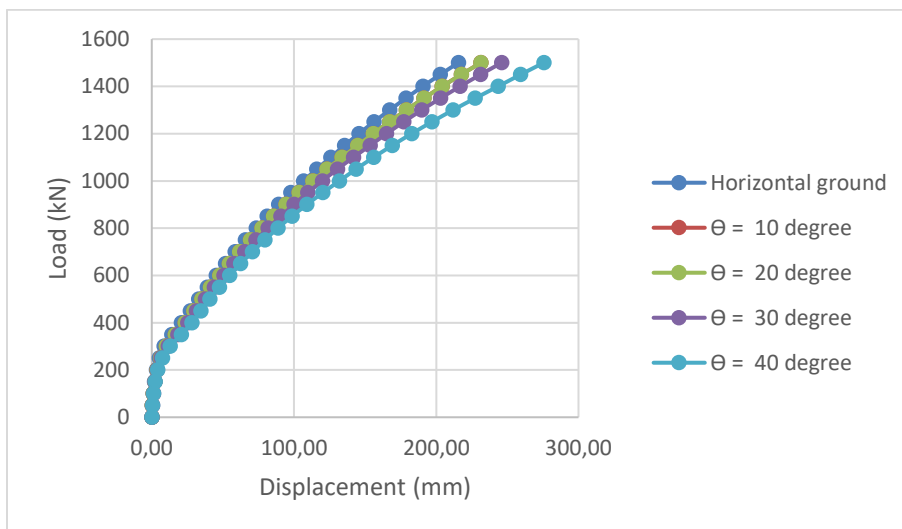


Figure 6: Lateral load – displacement variation for different slopes at zero edge distance

Figure 7 illustrates the effect of edge distance on displacement at the slope of 40° . When the slope starts at zero edge distance, the displacement is maximum and equal to 275.65 mm. It is higher by 27.9% than the level ground case. This is because at the slope of 40° , and zero edge distance, minimum soil is present on the sloping side to offer passive resistance. However, as the edge distance increases, more soil is available for the same slope, which causes lesser displacement. At edge distances of 2D, 5D, and 9D, the increase in displacement is 14.62 %, 5.32 %, and 0.48 %, respectively. The same trend is observed for other slopes also. However, for the lower slope, the variation in percentage increase is less. For 30° slope percentage decrease is 14.13 – 0.26 % for edge distances of 0-9D. It is 7.51 – 0.19 % for slope of 20° and 2.63 – 0.07 % for slope of 10° . **Figure 8 to Figure 10** depict the load-displacement variation for different edge distances at the slope of 30° , 20° , and 10° , respectively. The summary of displacements at a load of 1500 kN for all cases considered in the study is mentioned in **Table 2**.

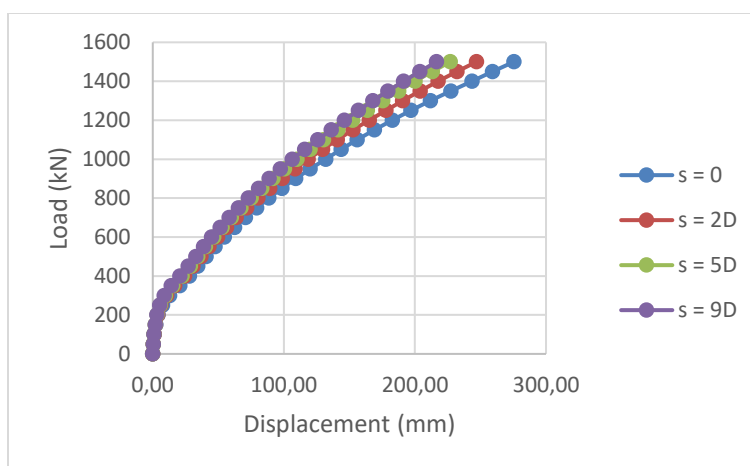


Figure 7: Lateral load – displacement variation for different edge distances at a slope of 40°

For the slope of 40° , the ultimate loads corresponding to 5 mm displacement at edge distances of zero, 2D, 5D, and 9D are less by 12.79%, 3.82%, 6.95%, and 0.84%, respectively, than the horizontal ground case. The ultimate loads predicted at 200 mm displacement are less by 12.34 %, 7.19 %, 2.73 %, and 0.25 %, respectively. A similar trend is observed for other slopes. It is observed that with an increase in edge distance, the pile group transforms into a stiffer nature, and the response in the ground with slope approaches the response in the horizontal ground. The ultimate loads obtained at 5 mm displacement and 200 mm displacement are reported in **Table 3** and **Table 4**, respectively.

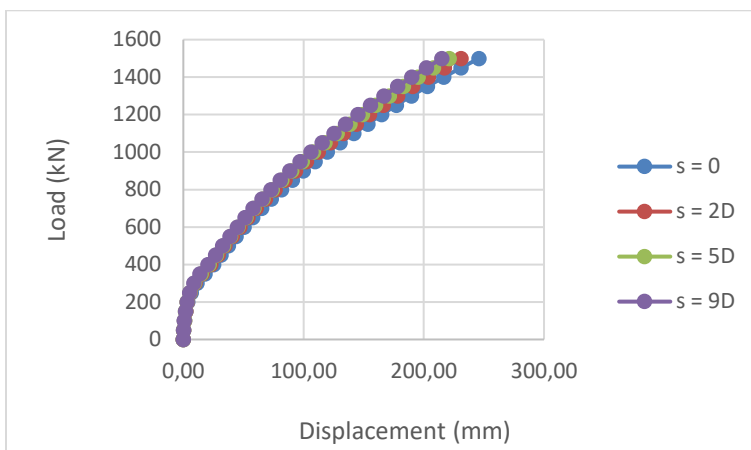


Figure 8: Lateral load – displacement variation for different edge distances at a slope of 30°

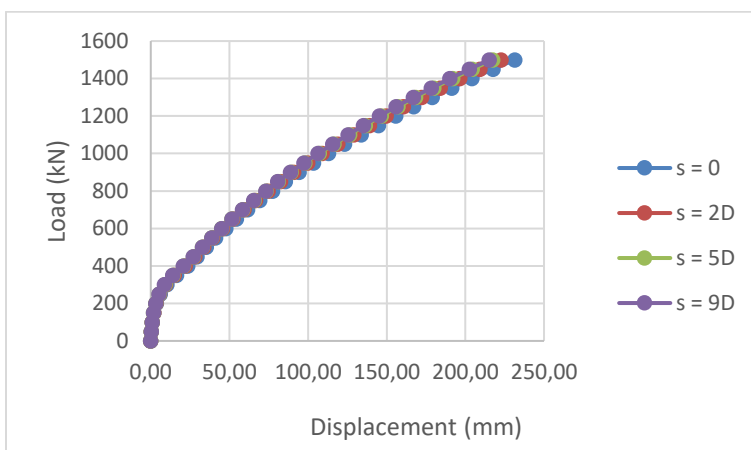


Figure 9 Lateral load – displacement variation for different edge distances at the slope of 20°

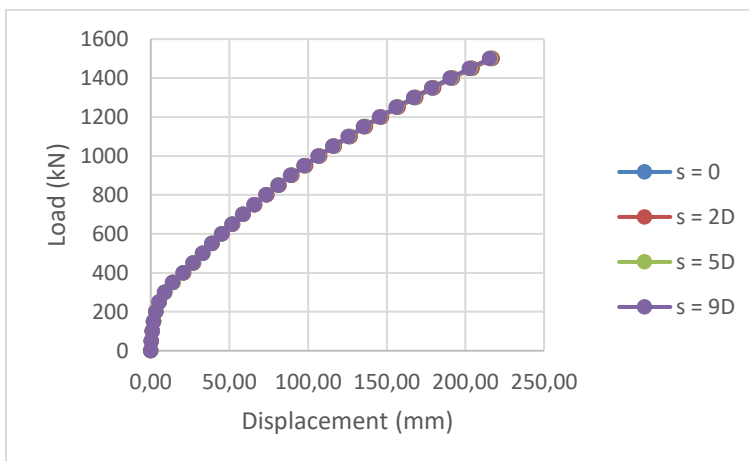


Figure 10 Lateral load – displacement variation for different edge distances at the slope of 10^0

	S = 0	S = 2D	S = 5D	S = 9D
Horizontal ground	215.52			
$\theta = 10^0$	221.19	217.01	216.98	215.66
$\theta = 20^0$	231.38	222.69	217.33	215.93
$\theta = 30^0$	245.97	231.16	221.16	216.08
$\theta = 40^0$	275.65	247.04	226.98	216.55

Table 2: Displacement for different slopes at different edge distances for the 2 x 2 pile group (P = 1500 kN)

	S = 0	S = 2D	S = 5D	S = 9D
Horizontal ground	244.02			
$\theta = 100$	237	240.51	242.45	243.78
$\theta = 200$	228.92	235.37	239.73	243.13
$\theta = 300$	220.42	230.29	236.89	242.65
$\theta = 400$	212.8	223.47	233.26	241.98

Table 3: Ultimate loads predicted for 5 mm displacement for the 2 x 2 pile group

	S = 0	S = 2D	S = 5D	S = 9D
Horizontal ground	1438.58			
$\theta = 10^0$	1418.04	1433.3	1436.94	1439.25
$\theta = 20^0$	1383.58	1413.54	1432.09	1439.68
$\theta = 30^0$	1338.53	1385.4	1418.29	1440.31
$\theta = 40^0$	1260.99	1335.16	1399.24	1434.99

Table 4: Ultimate loads predicted for 200 mm displacement for the 2 x 2 pile group

3.4. Bending Moments in Pile

Maximum bending moments generated in the front (G1) and rear pile (G2) are mentioned in **Table 5**.

In the rear pile, the highest bending moment is developed at the slope of 40° when the edge distance is zero. It is higher than the horizontal ground case by 10.16 %. As the edge distance is increased, the increase is observed to reduce. At the edge distance of 2D, 5D, and 9D, the increase is 9.08 %, 8.31 %, and 5.44 %, respectively. If the slope is reduced, the increase in the maximum bending moment also reduces. At zero edge distance, at the slope of 30° , 20° , and 10° the increase is 9.34 %, 8.81 %, and 8.53 %, respectively. A similar trend is observed in the maximum bending moment of the front pile. However, more bending moments are observed in the rear pile than in the front pile. This is because this pile is near to the slope, and less soil is available to offer passive resistance. At a slope of 10° , the maximum bending moment in the rear pile is higher than the front pile by 13.91 % at zero edge distance. This effect is intensified at the higher slope. The difference between 200, 300, and 400 is 14.17 %, 14.58 %, and 15.14%, respectively. For the same slope, as the edge distance increases, the difference is observed to reduce. For the slope of 40° , at edge distances of zero, 2D, 5D, and 9D, the difference is 15.14%, 14.95 %, 14.56 %, and 13.45 %, respectively.

Figure 11 and Figure 12 illustrate the comparison of bending moment variation along the depth of pile in a front pile and rear pile for two cases. The first case is in the horizontal ground, and the second is in the ground with a slope of 40° and an edge distance equal to zero. In both piles, the point of maximum bending moment is near the depth of 5 m in the horizontal ground case. This is the point of zero-shear. The passive resistance of the soil balances the horizontal load acting on the pile up to this point. In the sloping ground, less soil is available to offer passive resistance. Hence, the point of maximum bending moment shifts downward. In both piles, at a slope of 40° with zero edge distance, it shifts near a depth of 7m.

	Horizontal ground	S = 0	S = 2D	S = 5D	S = 9D
Pile G1					
$\theta = 10^\circ$	6618.51	6940.08	6779.15	6709.79	6678.54
$\theta = 20^\circ$		6942.30	6857.95	6818.77	6710.15
$\theta = 30^\circ$		6951.00	6879.58	6863.89	6753.86
$\theta = 40^\circ$		6969.61	6912.36	6886.51	6770.46
Pile G2					
$\theta = 10^\circ$	7284.57	7905.65	7812.61	7641.07	7483.58
$\theta = 20^\circ$		7926.38	7868.69	7708.15	7547.39
$\theta = 30^\circ$		7964.91	7901.92	7736.72	7614.77
$\theta = 40^\circ$		8024.51	7946.17	7889.77	7680.85

Table 5 Maximum bending moments for different slopes and edge distances for the 2 x 2 pile group (P=1500 kN)

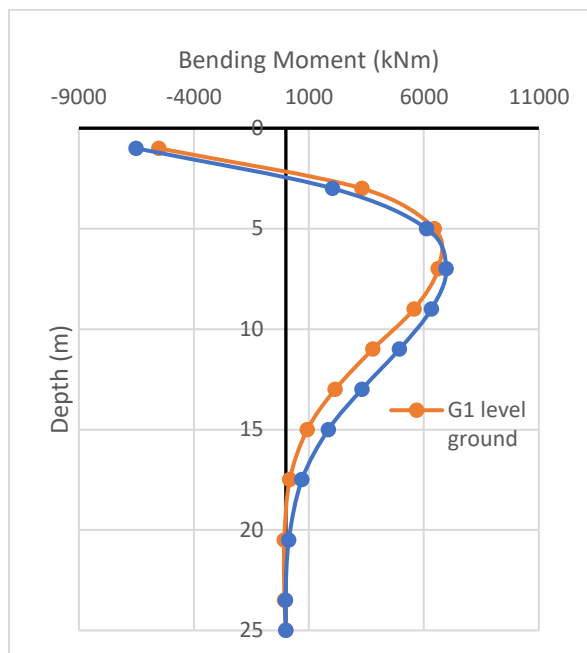


Figure 11: Comparison of bending moment along the depth in the front pile (G1), in level ground and at a slope of 40 degrees and edge distance equal to zero

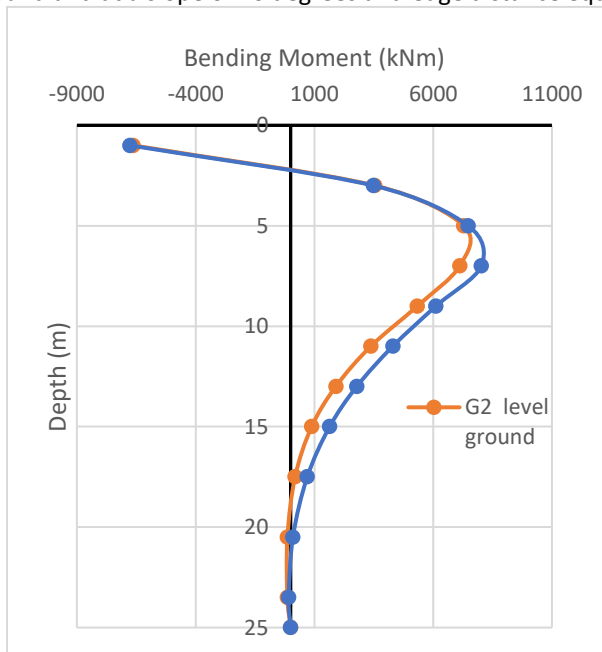


Figure 12: Comparison of bending moment along the depth in the rear pile (G2), in level ground and at a slope of 40 degrees and edge distance equal to zero

4. Conclusions

The present study aimed to explore the response of a laterally loaded 2 x 2 pile groups near a sloping ground using a numerical approach. The influence of slope angle and edge distance of the slope on the response of the pile group is investigated. Slopes of 10° , 20° , 30° , and 40° are considered, and analysis is carried out at the edge distance equal to zero, 2D, 5D, and 9D for each

slope. The maximum load applied is 1500 kN. As a basis for this study, an analysis of a 2 x 2 pile group in the horizontal ground is also carried out. The key findings of this study are mentioned below.

At the same edge distance, the lateral displacement also increases if the slope is increased. At zero edge distance, the displacement increases by 2.63 %, 7.36 %, 14.13 %, and 27.9 % for the slope of 10° , 20° , 30° , and 40° , respectively, compared to the horizontal ground case. If the edge distance is increased at the constant slope, the increase in displacement is found to decrease. At slope of 40° , for edge distance of zero, the 2D, 5D, and 9D displacements are higher by 27.9%, 14.62 %, 5.32 %, and 0.48 % respectively

The ultimate capacity of the pile group near the slope is less than in the level ground case. The maximum reduction of 12.79 % is observed at the slope of 40° with zero edge distance based on a 5 mm displacement criterion. The reduction in capacity is more for a higher slope. It decreases with an increase in edge distance. A similar trend in reduction is observed for the 5 mm and 200 mm displacement criteria.

The maximum bending moment of piles in the sloped ground is higher than the horizontal ground case. In the rear pile, at the slope of 40° with zero edge distance, the increase is by 10.16 %. At the edge distance of 2D, 5D, and 9D, the increase is 9.08 %, 8.31 %, and 5.44 %, respectively. In both piles, the pile response in terms of maximum bending moment in sloped ground approaches that of in horizontal ground with an increase in edge distance. However, the increase in edge distance required in a rear pile is more than a front pile to achieve this.

The maximum bending moments generated in the rear pile are higher than the front pile, even in the level ground case. This effect is increased in the sloping ground with an increase in slope. At angle of 10° , 20° , 30° and 40° the difference is 13.91 %, 14.17 %, 14.58 %, and 15.14%, respectively, at zero edge distance. With the increase in edge distance, the increase is found to reduce.

The point of zero shear force in a pile is deeper in the ground slope than in the horizontal ground case. In both piles, at the slope of 40° with zero edge distance, it is at 7 m, whereas in the horizontal ground case, it is at 5m.

References

- Basu, D., R. Salgado, and M. Prezzi. 2009. "A Continuum-Based Model for Analysis of Laterally Loaded Piles in Layered Soils." *Géotechnique* 59 (2): 127–40. <https://doi.org/10.1680/geot.2007.00011>.
- Chae, K. S., K. Ugai, and A. Wakai. 2004. "Lateral Resistance of Short Single Piles and Pile Groups Located near Slopes." *International Journal of Geomechanics* 4 (2): 93–103. [https://doi.org/10.1061/\(ASCE\)1532-3641\(2004\)4:2\(93\)](https://doi.org/10.1061/(ASCE)1532-3641(2004)4:2(93)).
- Chen, L., and H.G. Poulos. 1993. "Analysis of Pile-Soil Interaction under Lateral Loading Using Infinite and Finite Elements." *Computers and Geotechnics* 15 (4): 189–220. https://journals.scholarsportal.info/details/0266352x/v15i0004_c/189_aopiulluife.xml.
- Georgiadis, M., C. Anagnostopoulos, and S. Saflekou. 1992. "Cyclic Lateral Loading of Piles in Soft Clay." *GEOTECHNICAL ENGINEERING* 23 (1). <https://trid.trb.org/view/373350>.

- Indian Standard Code of Practice for Design and Construction of Pile Foundations. 1985. <https://ia600904.us.archive.org/22/items/gov.in.is.2911.4.1985/is.2911.4.1985.pdf>.
- IS 2911 (Part 4) -1985 (Reaffirmed 2010) Indian Standard Code of Practice for Design and Construction of Pile Foundations Part 4 Load Tests on Pile. Bureau of Indian Standard New Delhi
- Khatri, Bhishm Singh, and V. A. Sawant. 2020a. "Comparison of Lateral Response of Pile Group in Series and Parallel Arrangement near Sloping Ground." *International Journal of Geotechnical Engineering* 14 (6): 686–95. <https://doi.org/10.1080/19386362.2019.1617478>.
- Khatri, Bhishm Singh. 2020b. "Variation in Lateral Load Capacity of Pile Embedded near Slope with Ground Inclination and Edge Distance." *International Journal of Geotechnical Engineering* 14 (7): 740–51. <https://doi.org/10.1080/19386362.2018.1541149>.
- Mukherjee, Somenath, and Arindam Dey. 2019. "Analysis of Laterally Loaded Fixed-Headed Single Pile in Multilayered Soil Using P-Y Approach." In *Geotechnical Applications*, edited by Anirudhan I.V. and V.B. Maji, 13:41–50. Lecture Notes in Civil Engineering. Singapore: Springer Singapore. https://doi.org/10.1007/978-981-13-0368-5_5.
- Muthukkumaran, K., and N. Begum. 2009. "Experimental Investigation on Single Model Pile in Sloping Ground under Lateral Load." *International Journal of Geotechnical Engineering* 3 (1): 133–46. <https://doi.org/10.3328/IJGE.2009.03.01.133-146>.
- Muthukkumaran, K, R Deendayal, and T G Sitharam. 2015. "Response of Laterally Loaded Pile Groups in Sloping Ground."
- Muthukkumaran, K., R. Sundaravadivelu, and S.R. Gandhi. 2008. "Effect of Slope on P-Y Curves Due to Surcharge Load." *Soils and Foundations* 48 (3): 353–61. <https://doi.org/10.3208/sandf.48.353>.
- Nayak, Gyan C., and Olgierd C. Zienkiewicz. 1972. "Convenient Form of Stress Invariants for Plasticity." *Journal of the Structural Division* 98 (4): 949–54.
- Ng, Charles W. W., and L. M. Zhang. 2001. "Three-Dimensional Analysis of Performance of Laterally Loaded Sleeved Piles in Sloping Ground." *Journal of Geotechnical and Geoenvironmental Engineering* 127 (6): 499–509. [https://doi.org/10.1061/\(ASCE\)1090-0241\(2001\)127:6\(499\)](https://doi.org/10.1061/(ASCE)1090-0241(2001)127:6(499)).
- Potts, David M., Lidija Zdravković, Trevor I. Addenbrooke, Kelvin G. Higgins, and Nebojša Kovačević. 1999. *Finite Element Analysis in Geotechnical Engineering: Application*. Vol. 2. Thomas Telford London.
- Pourkhosravani, Amin, and Adel Asakereh. 2013. "Behavior of Laterally Loaded Piles in Cohesive Soil Slopes" 2 (23): 52–55.
- Prakash, Shamsher. 1962. "Behavior of Pile Groups Subjected to Lateral Loads." Ph.D. Thesis, University of Illinois at Urbana-Champaign.
- Rao, S. Narasimha, V. G. S. T. Ramakrishna, and M. Babu Rao. 1998. "Influence of Rigidity on Laterally Loaded Pile Groups in Marine Clay." *Journal of Geotechnical and Geoenvironmental Engineering* 124 (6): 542–49.
- Rollins, Kyle M., Kimball G. Olsen, Derek H. Jensen, Brian H. Garrett, Ryan J. Olsen, and Jeffery J. Egbert. 2006. "Pile Spacing Effects on Lateral Pile Group Behavior: Analysis." *Journal of*

- Geotechnical and Geoenvironmental Engineering 132 (10): 1272–83.
[https://doi.org/10.1061/\(ASCE\)1090-0241\(2006\)132:10\(1272\)](https://doi.org/10.1061/(ASCE)1090-0241(2006)132:10(1272)).
- Stewart, D.P., R.J. Jewell, and M.F. Randolph. 1993. “Numerical Modelling of Piled Bridge Abutments on Soft Ground.” *Computers and Geotechnics* 15 (1): 21–46.
[https://doi.org/10.1016/0266-352X\(93\)90015-Y](https://doi.org/10.1016/0266-352X(93)90015-Y).
- Tang, Xiaochao, and Minghui Yang. 2020. “Analysis of Laterally-Loaded Piles in Weathered Rock Slopes Based on p-y Curve Method.” *International Journal of Geotechnical Engineering* 14 (7): 809–19. <https://doi.org/10.1080/19386362.2018.1498199>.
- Terzaghi, Karl, and Ralph B. Peck. 1967. *Soil Mechanics in Engineering Practice*. 2nd ed. New York: John Wiley & Sons.
- Uncuoğlu, Erdal, and Mustafa Laman. 2011. “Lateral Resistance of a Short Rigid Pile in a Two-Layer Cohesionless Soil.” *Acta Geotechnica Slovenica* 8 (2): 19–43.
<https://avesis.erciyes.edu.tr/yayin/5491121f-7700-4375-b404-fc23f97564b3/lateral-resistance-of-a-short-rigid-pile-in-a-two-layer-cohesionless-soil>.
- Viladkar, M.N., J. Noorzaei, and P.N. Godbole. 1995. “Convenient Forms of Yield Criteria in Elasto-Plastic Analysis of Geological Materials.” *Computers & Structures* 54 (2): 327–37.
[https://doi.org/10.1016/0045-7949\(94\)E0199-C](https://doi.org/10.1016/0045-7949(94)E0199-C).